Bremsstrahlung from relativistic bare heavy ions: Nuclear and electronic contributions in amorphous and crystalline materials

Tue V. Jensen and Allan H. Sørensen
Department of Physics and Astronomy, University of Aarhus, DK-8000 Aarhus C, Denmark
(Received 21 December 2012; published 15 February 2013)

A charged particle emits bremsstrahlung while traversing matter. We calculate the radiation cross section for bare heavy ions penetrating amorphous materials and single crystals at highly relativistic energies. The main component originates in scattering of the virtual photons of screened target nuclei on the projectile. It appears at, approximately, 2γ times the energy of the giant dipole resonance of the projectile, approximately 25γ MeV for a lead nucleus ($\gamma \equiv E/Mc^2$, where E and M denote the projectile energy and mass). The emission pertains to relatively close impacts, with impact parameters ranging to, at maximum, the screening radius of the target atoms. As a result, the main bremsstrahlung component shows channeling dips, that is, dips in yield upon variation of the incidence angle to major crystallographic directions of a single crystal. The minimum yield increases with γ but saturates at a very low value. Incoherent interaction with single target electrons gives rise to two additional bremsstrahlung components, a modest component due to scattering of virtual photons of the electrons on the projectile and a strong low-energy component due to scattering of the virtual photons of the projectile on the electrons. The difference in radiation levels can be traced to the mass of the scatterer. Since target electrons are more widely distributed than nuclei in a crystal channel the variation of the electron component of the bremsstrahlung with incidence angle to a major crystallographic direction is less abrupt than the variation of the nuclear component. In consequence, the shape of the total bremsstrahlung spectrum changes when the crystal is tilted and the individual components may be singled out. Pair creation is also sensitive to the orientation of a crystalline material, resulting in a pronounced directional dependence of the energy loss of bare heavy ions at extreme relativistic energies.

DOI: 10.1103/PhysRevA.87.022902 PACS number(s): 34.50.Bw, 61.85.+p, 78.70.−g, 41.60.−m

I. INTRODUCTION

Bremsstrahlung is the major energy-loss channel for high-energy electrons. For relativistic heavy nuclei the requirement of coherent action of constituents limits bremsstrahlung to relatively soft photons, that is, photons of energy much less than the primary [1]. The implication is that, despite a series of previous claims, bremsstrahlung never dominates the energy loss for bare heavy ions penetrating matter. Instead, moderation is due to atomic excitation and ionization processes at moderate energies and electron-positron pair production at high energies, with transition 3 to 4 orders of magnitude above the projectile rest energy.

While not contributing in any significant way to the energy loss of relativistic bare heavy ions, the emitted bremsstrahlung reveals unique features related to the composite nature of the projectiles such as a resonance structure succeeded by an effective cutoff with increasing photon energy. This emerges in the main bremsstrahlung component corresponding to scattering of the virtual photons of target atoms on the projectile investigated in Ref. [1]. Additional components appear, the strongest being due to scattering of virtual photons of the projectile on target electrons. This "Compton component" has support essentially only at energies below the resonance in the main component. However, the intensity at low energies is so high that the Compton component contributes substantially more to the energy loss than the main component—albeit not changing the overall conclusion that bremsstrahlung never dominates the energy loss.

By selecting a single crystal as target and aiming the heavy ions near a low-index crystallographic direction the different components may be depleted or enhanced relative to each other by slightly tilting the crystal. That is, the shape of the bremsstrahlung spectrum may be controlled by the choice of angle of incidence. This unique option appears as a result of the governing of the projectile motion by many correlated small-angle scattering events with target atoms for sufficiently close alignment. The resulting channeling motion prevents projectiles from coming close to target nuclei, depleting the main bremsstrahlung component, but still leaves a fair chance for interaction with target electrons, which are more widely distributed in the crystal channels. The chance for creation of electron-positron pairs is also depleted. Hence the bremsstrahlung emitted by the secondaries which falls in the same energy range as the Compton component of the heavy-ion bremsstrahlung is reduced relative to the latter. The nonuniform projectile flux in the nearly aligned crystal further causes a substantial depletion of the energy loss of heavy ions at such high energies that loss to pair production dominates. We note that heavy ions from CERN's Large Hadron Collider (LHC) may be aimed at a bent crystal in the future in order to extract beams for fixed-target experiments [2]. If realized, this opens the possibility of channeling experiments with ultrarelativistic heavy ions.

In this paper we present a detailed investigation of the various contributions to bremsstrahlung emission by relativistic bare heavy ions penetrating matter. Interaction with target atoms and individual target electrons is considered separately, and depletion of the projectile intensity due to electromagnetic dissociation is included. In the first part of the paper the target is assumed to be amorphous. In the second part the heavy ions are aimed at a single crystal with a major crystallographic axis nearly aligned with the projectile beam. The variation

with the angle of incidence of the individual bremsstrahlung components, as well as their sum, is determined. We conclude with comments on electron-positron pair creation.

As in Ref. [1] we require the projectile to survive a given interaction as an entity in order to count the emitted electromagnetic radiation as bremsstrahlung. Throughout, we use Ze, M, and E for projectile charge, mass, and energy, while Z_t denotes the atomic number of the target and m is the electron mass. The Lorentz factor of the projectile $\gamma \equiv E/Mc^2$ is assumed to be about 100 or larger. A previous publication [3] gives a brief account of some of the results derived below.

II. BREMSSTRAHLUNG BY THE WEIZSÄCKER-WILLIAMS METHOD

Bremsstrahlung emitted by a bare heavy ion penetrating matter is conveniently calculated by means of the Weizsäcker-Williams (WW) method of virtual quanta. For a particle of charge q moving at constant velocity $\mathbf{v}$, close to the speed of light c, the energy transmitted per unit area and frequency ω by virtual photons at a point fixed at transverse distance b from the particle path amounts to

$$\frac{d^3I}{d\omega d^2b} = \frac{q^2}{\pi^2 cb^2}[xK_1(x)]^2, \tag{1}$$

where K_1 is a modified Bessel function [4]. The Lorentz factor is assumed to be sufficiently high throughout that terms of relative order $1/\gamma^2$ may be neglected. For a bare charged particle the parameter x is given as

$$x = \omega b/\gamma c. \tag{2}$$

Expression (1) holds also for a dressed particle of central charge q producing an exponentially screened Coulomb potential (Yukawa potential) in its rest frame; in this case x reads

$$x = \sqrt{(\omega b/\gamma c)^2 + (b/a)^2}, \tag{3}$$

where a is the screening length [1]. Since the modified Bessel function K_1 falls off exponentially for arguments larger than 1, the effective range in frequency for a given impact parameter, or in impact parameter at a given frequency, is determined by the condition $x = 1$.

The number $N_{\rm WW}$ of virtual photons traversing a unit area per photon-energy bin is obtained by dividing the energy spectrum, (1), by the energy of the individual photons, and the average number N_p of events of a given process, also differential in virtual photon energy, results by subsequently multiplying by the corresponding cross section. In bremsstrahlung a photon scattering cross section is applied. Depending on the contributing scattering process, this may be either a total cross section at the given photon energy, $\sigma_\gamma(\omega)$, or a cross section differential in photon scattering angle, $d\sigma_\gamma(\omega)/d\Omega$. For the former case, for instance,

$$\frac{dN_p(b)}{d\hbar\omega} = \frac{d^3N_{WW}}{d\hbar\omega d^2b}\sigma_\gamma(\omega) = \frac{1}{\hbar\omega}\frac{d^3I}{d\hbar\omega d^2b}\sigma_\gamma(\omega). \tag{4}$$

Also depending on the process, the energy of the scattered photon may or may not be equal to the incoming virtual photon energy. In the former case an expression like (4) directly gives the observable bremsstrahlung contribution; in the latter case an integration over those virtual photon energies which may result in a given scattered photon energy is to be added. In some cases the projectile has a significant chance of disintegrating or being removed due to other processes. One such process is electromagnetic dissociation, which causes breakup of the projectile with a high probability in very close encounters when both collision partners are heavy nuclei [5,6]. To account for this, $dN_p(b)/d\hbar\omega$ may be multiplied by a depletion factor $F(b) \leqslant 1$. For electromagnetic dissociation F is equal to the probability of no virtual photons participating in the photodissociation process, that is,

$$F(b) = P^0(b) = \exp\left(-\int d\hbar\omega\, \sigma_{\rm diss}(\hbar\omega)\frac{1}{\hbar\omega}\frac{d^3I_t}{d\hbar\omega d^2b}\right), \tag{5}$$

where $\sigma_{\rm diss}$ is the cross section for dissociation of the projectile upon photon impact and the virtual photon intensity is that due to the target atom and encountered by the projectile in its rest frame.

When much smaller than unity, the average number of events of a process in a given range of photon energies provides the probability of the process occurring in this range. For an even distribution of the relative position of projectile and target objects, we introduce the cross section pertaining to the process as this probability integrated over all impact parameters. Below we operate with the so-called radiation cross section $d\chi/d\hbar\omega$ obtained by including an extra factor of $\hbar\omega$. Hence

$$\frac{d\chi}{d\hbar\omega} = \hbar\omega\int d^2b\frac{dN_p(b)}{d\hbar\omega}F(b) = \int d^2b\frac{d^3I}{d\hbar\omega d^2b}\sigma_\gamma(\omega)\,F(b). \tag{6}$$

The radiation cross section carries the dimension of an area and is sometimes alternatively termed the power spectrum. In cases where $F(b) = 1$ at all b the impact parameter dependence derives solely from the virtual photon intensity, (1). Computation of the cross section rather than the average number of events at a given b then simply implies substitution of Eq. (1) by the total intensity obtained by integration of Eq. (1) over all impact parameters beyond a certain minimum $b_{\rm min}$ to be decided on. This total intensity reads [4]

$$\frac{dI}{d\hbar\omega} = \frac{2}{\pi}\alpha(q/e)^2\left\{\xi K_0(\xi)K_1(\xi) + \frac{1}{2}\xi^2\left[K_0^2(\xi) - K_1^2(\xi)\right]\right\}, \tag{7}$$

where ξ is given as x, Eq. (2) or (3), with b replaced by its minimum $b_{\rm min}$, and $\alpha = e^2/\hbar c$ is the fine-structure constant. In many applications we have $\xi \ll 1$, whereby the intensity, (7), reduces to

$$\frac{dI}{d\hbar\omega} = \frac{2}{\pi}\alpha(q/e)^2\left\{\ln\frac{1.123}{\xi} - \frac{1}{2}\right\} \equiv \frac{2}{\pi}\alpha(q/e)^2\ln\frac{C}{\xi}. \tag{8}$$

The last transcription is introduced for later convenience, $C \equiv 2/\exp(\gamma_E + \frac{1}{2}) = 0.681\ldots$, where $\gamma_E = 0.5772\ldots$ is Euler's constant. With $F \equiv 1$ the radiation cross section is simply the product of the total virtual intensity, Eq. (7) or (8),

and the photo cross section,

$$\frac{d\chi}{d\hbar\omega} = \frac{dI}{d\hbar\omega}\,\sigma_\gamma(\omega), \quad F \equiv 1. \tag{9}$$

There are four contributions to the bremsstrahlung emitted when a bare heavy ion penetrates matter. The main contribution for $\gamma \gg 1$ is due to scattering of the virtual photons of screened target nuclei on the projectile in the rest frame of the latter. The other three are (i) scattering of the virtual photons of the projectile on target nuclei, (ii) scattering of the virtual photons of the projectile on individual target electrons, and (iii) scattering of the virtual photons of individual target electrons on the projectile in its rest frame. We examine each of these contributions below.

A. Interaction with target nuclei

1. Main component

Bremsstrahlung due to scattering of the virtual photons of a screened target nucleus on the penetrating projectile is discussed in detail in Ref. [1]. The main points are as follows: The requirement for coherent action of the constituents of the projectile nucleus in order to prevent breakup translates into application of the cross section for elastic photon scattering. Since the photon energy in the laboratory depends on the scattering angle in the rest frame $\mathcal{R}$ of the projectile, a cross section differential in scattering angle is needed. For a ^{208}Pb projectile it may be approximated as

$$\frac{d\sigma_\gamma}{d\Omega'} = Z^2 r_p^2 \frac{1}{2}(1+\cos^2\psi') \times \begin{cases} \left(\frac{ZM_p}{M}\right)^2, & \hbar\omega' < \hbar\omega_1 \\ 0.793\,\frac{(\hbar\omega')^4}{((\hbar\omega')^2-(E_m)^2)^2+(\Gamma\hbar\omega')^2}, & \hbar\omega_1 < \hbar\omega' < \hbar\tilde{\omega}_2 \\ 1.93\,\exp\left(-\epsilon(\hbar\omega'-\hbar\tilde{\omega}_2)\sin^2\frac{\psi'}{2}\right), & \hbar\tilde{\omega}_2 < \hbar\omega' \end{cases}. \tag{10}$$

Here $r_p \equiv e^2/M_p c^2$ is the classical radius of the proton of mass M_p; for lead $Z^2 r_p^2 = 0.1584$ mb. The parameters for the central region, which mirrors the giant dipole resonance, are $E_m = 13.7$ MeV and $\Gamma = 4.15$ MeV, and the value of the high-energy depletion factor is $\epsilon = 0.11\ \text{MeV}^{-1}$. The dividing energies are $\hbar\omega_1 = 7.69$ MeV and $\hbar\tilde{\omega}_2 = 22.0$ MeV. Primes denote quantities given in $\mathcal{R}$. In particular, ψ' is the photon scattering angle measured relative to $-\mathbf{v}$, whereby the photon emission angle relative to $\mathbf{v}$ is $\theta' = \pi - \psi'$. The product of the virtual photon intensity of the screened target nucleus in $\mathcal{R}$ and the scattering cross section produces the differential radiation cross section in the projectile rest frame,

$$\frac{d^4\chi'}{d\hbar\omega' d\Omega' d^2b} = \frac{d\sigma_\gamma}{d\Omega'}\frac{d^3I'}{d\hbar\omega' d^2b}. \tag{11}$$

Transformation from $\mathcal{R}$ to the laboratory may be performed by the use of invariance of the quantity on the left-hand side of Eq. (11) divided by the square of the photon frequency. Emission angles are generally small in the latter, $\gamma\theta \sim 1$, which allows for a small-angle approximation. Combined, we get

$$\frac{d^4\chi}{d\hbar\omega d\Omega d^2b} = \frac{16}{3}\alpha Z_t^2 Z^2 r_p^2 \frac{3\gamma^2(1+\gamma^4\theta^4)}{4\pi^2(1+\gamma^2\theta^2)^4}\frac{1}{b^2} \times [x' K_1(x')]^2\ \Xi\ F(b), \tag{12}$$

where the quantity Ξ is the factor in curly brackets in the scattering cross section, Eq. (10), with the frequency and emission angle expressed by their laboratory values:

$$\omega' \simeq \frac{1+\gamma^2\theta^2}{2\gamma}\omega, \quad \sin^2\frac{\psi'}{2} \simeq \frac{1}{1+\gamma^2\theta^2}. \tag{13}$$

In the argument $x' = [(\omega' b/\gamma c)^2 + (b/a)^2]^{1/2}$, Eq. (3), the first relation in Eq. (13) is similarly applied for ω'. The minimum value of the impact parameter is the sum of the projectile and target nuclear radii, $b_{\min} = R_\Sigma \equiv R + R_t$, in order to keep the projectile intact (no breakup). For the screening length we substitute the Thomas-Fermi distance, $a = a_{\text{TF}} = 0.885 a_0 Z_t^{-1/3}$, where a_0 is the Bohr radius of hydrogen. As an extension of Ref. [1], the factor $F(b)$ is included in Eq. (12) to allow for depletion due to electromagnetic dissociation or similar processes. In the applications below we are not interested in details of the angular distribution. Accordingly, an integration over emission angles is performed. The structure of approximation (10) to the scattering cross section implies up to three contributing ranges of photon emission angles for any fixed photon energy in the laboratory. Due to the transformation from the projectile rest frame to the laboratory, the radiation cross section peaks near 2γ times the energy of the giant dipole resonance, that is, approximately at 25γ MeV for a lead projectile. For lighter projectiles the peak will be positioned at a higher energy, and for heavier projectiles at a slightly lower energy, since the giant dipole resonance moves from roughly 19 MeV for nuclei with about 50 nucleons to approximately 13 MeV for the heaviest nuclei; data and useful fits may be found in Ref. [7].

We do not need the radiation cross section differential in impact parameter for incidence in an amorphous medium (or "random" incidence in a crystal). In cases with depletion, $F(b) < 1$, the integration of the cross section, (12), over the impact parameter is performed numerically. Otherwise, provided the depletion factor $F(b)$ is close to unity and the average number of events $N_p(b)$ is small at all impacts, we may apply the integrated spectrum of virtual photons, (7), rather than Eq. (1). Since this spectrum extends far beyond frequencies where the scattering cross section has support, the asymptotic form, (8), is a fine approximation. Accordingly, the radiation cross section assumes the form

$$\frac{d^2\chi}{d\hbar\omega d\Omega} = \frac{16}{3}\alpha Z_t^2 Z^2 r_p^2 \frac{3\gamma^2(1+\gamma^4\theta^4)}{2\pi(1+\gamma^2\theta^2)^4}\ln\left(\frac{C}{\xi'}\right)\Xi, \quad F \equiv 1, \tag{14}$$

where $\xi' = [(\omega' R_\Sigma/\gamma c)^2 + (R_\Sigma/a_{\rm TF})^2]^{1/2}$ when the minimum impact parameter and screening length are chosen as above. Again, the first relation in Eq. (13) has to be applied for ω'. An integration over emission angles produces the radiation cross section $d\chi/d\hbar\omega$.

2. *Low-energy component*

Scattering of virtual photons of the projectile on target nuclei brings a relatively small amount of radiation at most energies. Due to the lack of a Lorentz boost, bremsstrahlung contributions of this type are only substantial for photon energies near the giant dipole resonance, which is a factor of 2γ below the peak in the spectrum of the main component described above. The differential radiation spectrum is obtained by multiplying Eq. (4) by the photon energy; that is,

$$\frac{d^3\chi}{d\hbar\omega d^2b} = \frac{Z^2\alpha}{\pi^2 b^2}\left[\frac{\omega b}{\gamma c}K_1\left(\frac{\omega b}{\gamma c}\right)\right]^2 \sigma_\gamma(\omega)\, F(b). \quad (15)$$

We have applied Eqs. (1) and (2) for the bare projectile, and a depletion factor is again included. For a lead target we may determine $\sigma_\gamma(\omega)$ from the approximation to the differential scattering cross section, Eq. (10), without primes and with Z and M substituted by Z_t and the mass of the target nucleus, M_t, respectively. Integration over all scattering angles yields

$$\sigma_\gamma = \frac{8\pi}{3} Z_t^2 r_p^2 \times \begin{cases} \left(\frac{Z_t M_p}{M_t}\right)^2, & \hbar\omega < \hbar\omega_1 \\ 0.793\frac{(\hbar\omega)^4}{((\hbar\omega)^2-(E_m)^2)^2+(\Gamma\hbar\omega)^2}, & \hbar\omega_1 < \hbar\omega < \hbar\tilde{\omega}_2 \\ 1.93\, f(\epsilon(\hbar\omega-\hbar\tilde{\omega}_2)), & \hbar\tilde{\omega}_2 < \hbar\omega \end{cases}, \quad (16)$$

where

$$f(x) = \frac{3}{2x^3}[x^2 - 2x + 4 - e^{-x}(x^2+2x+4)]. \quad (17)$$

Note that $f(0) = 1$, $f(x)$ approaches $3/2x$ at high x values and that the cross section, (16), varies continuously with the photon energy.

Strictly speaking, since we consider scattering on the target nucleus there is no reason to require no breakup and restrict to coherent action of the nuclear constituents. However, since the incoherent component scales linearly with Z_t, whereas the coherent component scales as Z_t^2 and generally includes a resonance, it brings only a small correction, in particular, for heavy target elements. Hence the incoherent contribution is ignored. See also comments in Sec. II C.

In cases where we may neglect depletion, $F(b) \equiv 1$, we may immediately write down the integral of Eq. (15) over all impact parameters larger than the sum of the nuclear radii:

$$\frac{d\chi}{d\hbar\omega} = \frac{2}{\pi}\alpha Z^2 \ln\left(\frac{C\gamma c}{\omega R_\Sigma}\right)\sigma_\gamma(\omega). \quad (18)$$

As before we have applied the asymptotic form of the virtual photon spectrum since the argument ξ appearing in Eqs. (7) and (8) is much smaller than 1 for frequencies where the cross section, (16), is appreciable when $\gamma \gtrsim 100$: for lead ions on a lead target the cutoff implied when the argument in the logarithm of Eq. (18) reaches the value 1 is $\gamma \times 9.6$ MeV, which, for our standard case of $\gamma = 170$, amounts to 1.6 GeV, at which value the cross section, (16), is reduced to 0.002 times its maximum value.

Note that the exponential extinction of the virtual-photon intensity appears before the peak of the main contribution, near 25γ MeV for a lead ion, is reached. Hence no processes involving scattering of the virtual photons of the projectile contribute around or beyond the peak.

B. Interaction with target electrons

1. *Scattering of virtual photons of the projectile on electrons*

Bremsstrahlung is also emitted as virtual photons corresponding to the projectile field scatter off individual target electrons. The process is Compton scattering (except perhaps for sufficiently low frequencies at which atomic binding plays a role). If we aim for the energy-loss spectrum, that is, the energy lost to both photon emission and electron recoil, we may simply substitute the total cross section for $\sigma_\gamma(\omega)$ in Eq. (4); that is,

$$\sigma_\gamma(\omega) = 2\pi r_e^2 Z_t\left(\frac{1+\eta}{\eta^3}\left[\frac{2\eta(1+\eta)}{1+2\eta} - \ln(1+2\eta)\right] + \frac{1}{2\eta}\ln(1+2\eta) - \frac{1+3\eta}{(1+2\eta)^2}\right), \quad \eta \equiv \hbar\omega/mc^2, \quad (19)$$

where $r_e \equiv e^2/mc^2$ is the classical electron radius [8]. A factor of Z_t is included since we operate with cross sections per atom (rather than per electron).

In the Compton process the energy of the scattered photon is generally less than that of the incoming photon due to electron recoil. Hence when we aim for the spectrum of radiated photons the cross section in Eq. (4) should be that of a photon of higher energy $\hbar\omega_0$ to scatter into a photon of the requested energy $\hbar\omega$, and an integration over all energies $\hbar\omega_0 > \hbar\omega$ should be included. In place of Eq. (4) we then have

$$\frac{dN_p(b)}{d\hbar\omega} = \int_{\hbar\omega}^{\hbar\omega_{\rm max}} d\hbar\omega_0 \frac{1}{\hbar\omega_0}\frac{d^3I}{d\hbar\omega_0 d^2b}\frac{d\sigma_\gamma}{d\hbar\omega_0}(\omega_0 \to \omega), \quad (20)$$

where the maximum $\hbar\omega_{\rm max}$, determined by kinematics, is infinite unless very low energies are considered [$\hbar\omega < mc^2/2$, in which case $\hbar\omega_{\rm max} = \hbar\omega/(1 - 2\hbar\omega/mc^2)$]. Heitler gives the Compton cross section differential in final photon energy [8]; transcription to a cross section differential in initial energy involves an extra factor of $(\hbar\omega/\hbar\omega_0)^2$, hence

$$\frac{d\sigma_\gamma}{d\hbar\omega_0} = Z_t \pi r_e^2 mc^2 \frac{(\hbar\omega)^2}{(\hbar\omega_0)^4}\left[\frac{\hbar\omega_0}{\hbar\omega} + \frac{\hbar\omega}{\hbar\omega_0} + \left(\frac{mc^2}{\hbar\omega} - \frac{mc^2}{\hbar\omega_0}\right)^2 - 2mc^2\left(\frac{1}{\hbar\omega} - \frac{1}{\hbar\omega_0}\right)\right]. \quad (21)$$

The differential radiation cross section $d^3\chi/d\hbar\omega d^2b$ is obtained by multiplying Eq. (20) through by $\hbar\omega$.

Except for the reference frame, the process considered is nothing but bremsstrahlung for an electron penetrating the field of an atomic nucleus at rest: Application of the virtual photon method to the computation of electronic bremsstrahlung involves the exact same components as above

but is supplemented by a final transformation from (the original) rest frame of the electron to the laboratory frame (which, in ordinary electronic bremsstrahlung, is the rest frame of the nucleus) [4]. Hence the effective minimum impact parameter is the same. In the relativistic case the effective minimum impact parameter for virtual photons of the projectile scattering off target electrons is half the Compton wavelength of the electron, $b_{\min} = \lambda\!\!\!^{-}_C/2 \equiv \hbar/2mc$. This implies that the virtual photon spectrum extends effectively up to a maximum of approximately $\hbar\omega_0 = 2\gamma mc^2$ reached at the minimum impact parameter and corresponding to $x = 1$ in Eqs. (1) and (2). The characteristic photon-emission angle is inferable from the expression for the cross section differential in scattering angle given by Heitler [8]. For photon energies well above mc^2 it amounts to $\sqrt{2mc^2/\hbar\omega_0}$, which reduces to $1/\sqrt{\gamma}$ at the effective maximum of the virtual photon spectrum.

2. *Scattering of virtual photons of electrons on the projectile*

The calculation of bremsstrahlung due to scattering of virtual photons of target electrons on the projectile is similar to that of the main component. For the individual electron the virtual photon intensity is reduced by $1/Z_t^2$ relative to that appearing in the determination of the main component. The minimum impact parameter $b_{\min}$ is determined by the wave nature of the source of the virtual photons *viz* the electron and the size of the struck system, that is, $b_{\min}$ is the larger of the de Broglie wavelength of the electron in the rest frame of the projectile and the nuclear radius of the latter, $b_{\min} = \max\{R,\hbar/\gamma mv\} = \max\{R,\lambda\!\!\!^{-}_C/\gamma\}$ (with c substituted for v). For a lead projectile $b_{\min} = R$ for $\gamma \gtrsim 55$. Since the minimum impact parameter is of the same order of magnitude as that for the main component and only enters into the argument of a fairly large logarithm, bremsstrahlung due to scattering of the virtual photons of the target electrons amounts to essentially Z_t^{-1} times the main contribution.

3. *Jankus' radiative corrections*

Many years back, Jankus published an account on radiative corrections to the Bethe-Bloch formula for the stopping power of heavy particles penetrating matter [9]. The Bethe-Bloch formula concerns the energy loss due to collisional excitation and ionization of target atoms (see Sec. II C). Jankus includes (a) the emission of real photons of any energy in interactions with target electrons as well as (b) Schwinger's correction [10] to the elastic electron-scattering cross section due to emission and reabsorption of virtual photons and the emission of real soft photons. For the former part, Jankus considers collisions in the rest frame of the heavy particle and the energy loss in the laboratory frame is obtained by subsequent Lorentz transformation of the rest-frame values of energy and momentum transfers. Calculated in this way, the energy loss of the heavy particle is the sum of the energy transferred to both photons and electrons. Hence, it is not clear that Jankus' result simply adds to the Bethe-Bloch formula. For low- and moderate-momentum transfers q the calculation of contribution (a) is based on the standard Bethe-Heitler bremsstrahlung cross section [8]; for high-momentum transfers Schiff's result [11] is applied. However, Jankus does not follow Schiff's suggestion to include a form factor to account for finite nuclear size. This is a serious limitation for the collision energies of interest here. Finite nuclear size is also not included in the Schwinger correction. This renders the result inappropriate for our collision systems where the (positive) high-q and the (negative) Schwinger corrections in Jankus' calculation both are much larger numerically than the low-q correction. Hence we do not engage in a detailed comparison below of Jankus' results (neither the total nor the low-q result) with our result for the energy loss due to the Compton process.

We may add that for bare lead ions penetrating matter at $\gamma = 170$, Jankus' result corresponds to a correction to the stopping number L, introduced below, of $\Delta L \simeq 0.25$. The experiment in Ref. [12] reported deviations from collision theory increasing from $\Delta L = 0.30$ to $\Delta L = 0.73$ for targets of atomic numbers Z_t increasing from 6 to 82, with errors in the range 0.5%–1.0% corresponding to $\Delta L = 0.07$–0.14. For $Z_t \geqslant 50$, the recorded deviations fit almost perfectly with the contribution from electron-positron pair creation [13,14], with essentially no room left for Jankus' correction. For $Z_t \leqslant 29$, pair production does not fully account for the observed deviation and the experiment may seem not to rule out Jankus' correction in these cases. However, since Jankus' result is independent of the target when expressed in terms of ΔL, the experimental findings for the heavy targets basically rule out his result for all materials.

C. Results

Figure 1 shows the main bremsstrahlung component calculated as described in Sec. II A 1 for what is our standard case in the following: bare lead ions penetrating a lead target at $\gamma = 170$. The curve reaching the highest is produced by application of the photon intensities, (7) and (8), which obtain when no depletion of the primary intensity is included, $F \equiv 1$. The solid curve results when we require the projectile not to

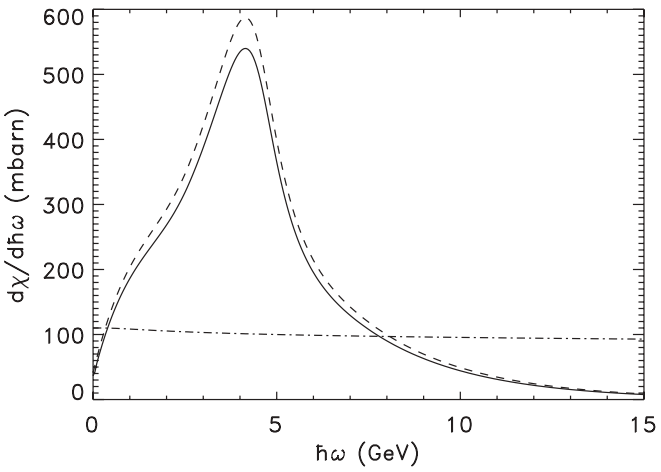

FIG. 1. Main component of the bremsstrahlung spectrum for bare ^{208}Pb ions penetrating a lead target at $\gamma = 170$. The dashed curve resulted from neglect of depletion due to electromagnetic dissociation of the projectile. Inclusion of such depletion produces the solid curve. The dot-dashed curve displays the radiation cross section for the hypothetical situation where both nuclei involved in a collision are pointlike and structureless.

dissociate in the collision with the target nucleus, that is, the depletion factor, (5), is included. The reduction in the main bremsstrahlung component is at the level of 8%, in agreement with the claim in Ref. [1]. For comparison Fig. 1 also displays the bremsstrahlung intensity which would result had the projectile been pointlike and structureless. While this is rather flat and extends to the primary kinetic energy, the actual spectrum shows a resonance structure which peaks at about 25γ MeV and is followed by a rather rapid falloff on the high-energy side. As demonstrated in Ref. [1] the main bremsstrahlung component maintains its position on the energy axis, and essentially also its shape, when plotted as a function of $\hbar\omega/\gamma$, whereas the intensity level increases with increasing value of γ until it saturates due to screening at a level about 40% above that shown in Fig. 1. When saturation over the entire spectrum is reached, screening is said to be complete. In general, screening is decisive at virtual photon frequencies such that the second term dominates the square root in Eq. (3), which, with the Thomas-Fermi length selected for a, corresponds to frequencies below $\gamma Z_t^{1/3} \times 4.2$ keV. For our standard case this is 3.1 MeV, which is well below the giant dipole resonance, implying that screening is of no importance. On the other hand, if γ is increased to 3000, the estimate reaches 55 MeV, which is about 4 times the giant dipole resonance peak whereby screening is essentially complete.

The probability of surviving a noncontact collision without dissociation, applied as the depletion factor F above, is calculated as described in Ref. [5]. Figure 2 displays the variation of this probability with the impact parameter for lead ions in lead and silicon targets. For lead targets the dissociation probability is high when the colliding nuclei are just about to touch. However, it falls to near 0 when the impact parameter is just 10 times larger. This is the reason for the modest reduction displayed in Fig. 1. For silicon the probability of dissociation

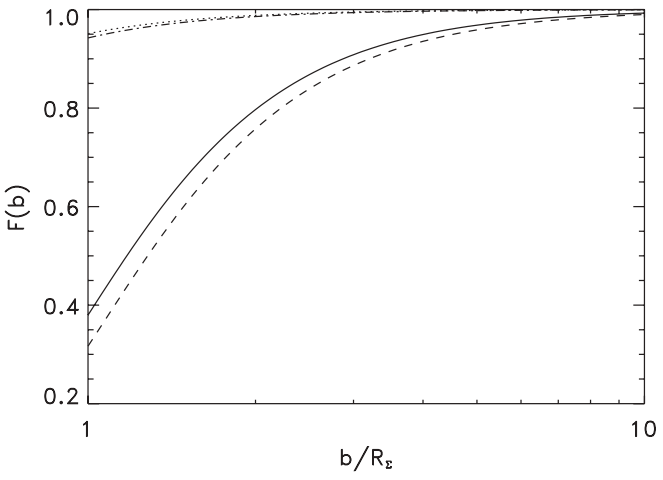

FIG. 2. Depletion factor $F(b)$ for a lead projectile due to electromagnetic dissociation. The two lower curves apply to a lead target (neutral atoms), with the solid curve corresponding to $\gamma = 170$ and the dashed curve to $\gamma = 3000$. The two upper curves apply to a silicon target (neutral atoms) at the same values of γ as for lead and with the same ordering. The impact parameter is shown in units of its minimum without nuclear contact *viz* the sum of the nuclear radii R_Σ.

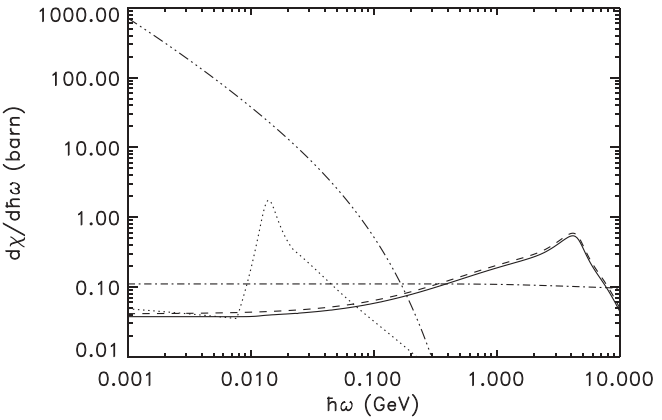

FIG. 3. Bremsstrahlung for bare ^{208}Pb ions penetrating a lead target at $\gamma = 170$. Bremsstrahlung due to scattering of the virtual photons of the projectile on target nuclei is shown by the dotted curve. The component corresponding to scattering on target electrons is shown by the triple-dot–dashed curve. The remaining curves are repeated from Fig. 1.

remains below 5%–6% at all impact parameters and hence has essentially no influence on the bremsstrahlung spectra resulting upon integration over impact parameters.

Above, the screening function of target atoms was approximated by a simple exponential with a screening length equal to the Thomas-Fermi length. This is obviously a rather rough approximation. A considerable improvement is obtained by applying the so-called Molière approximation, where the screening function appears as a sum of three exponentials [15]. However, the impact on the bremsstrahlung spectra is modest, typically not beyond 2%–3% for heavy targets.

Figure 3 shows the various bremsstrahlung components for our standard case on a logarithmic scale. The main component is repeated from Fig. 1 along with the reference curve for pointlike and structureless objects. The Compton-scattering component appears at low energies, way below the peak in the main bremsstrahlung component. It increases beyond both the reference curve and the main component with decreasing photon energy, starting at about 200 MeV. The Compton component further dominates the component due to scattering of virtual photons of the projectile on the target nucleus, implying that this component, which appears around the giant dipole resonance of the target nucleus, is of no practical importance. Bremsstrahlung due to scattering of the virtual photons of target electrons on the projectile adds about 1% $(1/Z_t)$ to the main component and is not shown in Fig. 3.

A depletion factor due to electromagnetic dissociation of the projectile is included in Fig. 3 for the main bremsstrahlung component. In principle, a depletion factor should be included in the Compton component as well. However, since depletion is confined to quite close encounters between the two nuclei, Fig. 2, while the virtual photon intensity peaks near the struck object, Eq. (1), which in the case of electrons is distributed over much larger distances to the target nucleus, depletion is neglected for the Compton component.

As mentioned in Sec. II A2, emission of radiation also results from incoherent scattering of virtual photons of the projectile on individual constituents of target nuclei. As a rough approximation we may compute this as Thomson

scattering on independent protons, Z_t for each target nucleus, for virtual photons with a wavelength shorter than the nuclear radius. The resulting intensity spectrum is rather flat, extending from a lower limit of 25–30 MeV for the heaviest nuclei up to the effective cut in the virtual photon intensity somewhat below the peak in the main bremsstrahlung component (cf. Sec. II A 2). For our standard case the incoherent component basically vanishes beyond 1.6 GeV and has a level of 1 mb at 200 MeV, which is 2 orders of magnitude below the main as well as the Compton component. Hence the incoherent component may safely be ignored.

Copious electron-positron pairs are generally produced in heavy-ion collisions. In Ref. [1] we discussed the significance, relative to the main component of the heavy-ion bremsstrahlung, of the bremsstrahlung emitted when the electron and the positron travel through the remaining part of the target following a pair-creation event. The pair-production cross section falls off beyond γmc^2 roughly as the inverse cube of the total energy of the pair and peaks well below this value [16,17], and the emitted bremsstrahlung extends to the kinetic energy of the emitting particle. In consequence, the radiation falls in the same energy range as the Compton component for the heavy particle. But since emission following pair production is a secondary process the dependence on the target thickness will be different and extraction is possible experimentally by varying the target thickness. For lead ions incident on a lead target the energy loss to electron-positron pairs is larger than that to the Compton component of bremsstrahlung for γ values beyond 10^2 (see Fig. 5). Hence elimination of bremsstrahlung from pairs requires targets that are thin compared to the radiation length. In crystals additional opportunities for elimination exist (see Sec. III D). For targets of lower atomic numbers the Compton component is relatively more important, due to slower scaling with Z_t, than the pair-creation component and the radiation length is longer.

Radiation is also emitted internally in the pair-creation process. This radiation is confined to low energies [18] and hence of no concern near the peak of the main bremsstrahlung component [19]. It is also small compared to the Compton component: with two photon-electron vertices and one electron-nucleus scattering vertex the cross section for a virtual photon to convert to an electron-positron pair plus an outgoing photon is, in order of magnitude, $Z_t^2\alpha^4$ (in units of the square of the Compton wavelength of the electron), whereas the cross section for Compton scattering, in order of magnitude, amounts to $Z_t\alpha^2$ (per target atom and in the same units). The ratio of the two is hence estimated as $Z_t\alpha^2$, which is lower than α, and in consequence, radiation emitted during electron-positron pair creation may be neglected.

It is important to note that the positions of the different contributions to the bremsstrahlung spectrum scale differently with γ. The position of the main contribution as well as that of the contribution due to scattering of the virtual photons of target electrons on the projectile shifts essentially in proportion to γ. The Compton contribution moves around at a slower pace. The contribution due to scattering of the virtual photons of the projectile on the target nucleus remains stationary around the giant dipole resonance of the latter. A simple formula for the γ dependence of the Compton component has not been found. Figure 4 shows how the photon energy at which the cross section for this component assumes a fixed preset value varies with γ for bare lead nuclei penetrating a lead target. The lowest cross section selected corresponds closely to the reference value in Figs. 1 and 3; that is, the solid curve in Fig. 4 essentially shows the variation with γ of the photon energy at which the Compton component (triple-dot-dashed curve in Fig. 3) and the reference curve (dot-dashed curve in Fig. 3) cross. This photon energy increases by about 2 orders of magnitude over the displayed 4-order-of-magnitude change in γ. For higher cross sections the photon energy varies less.

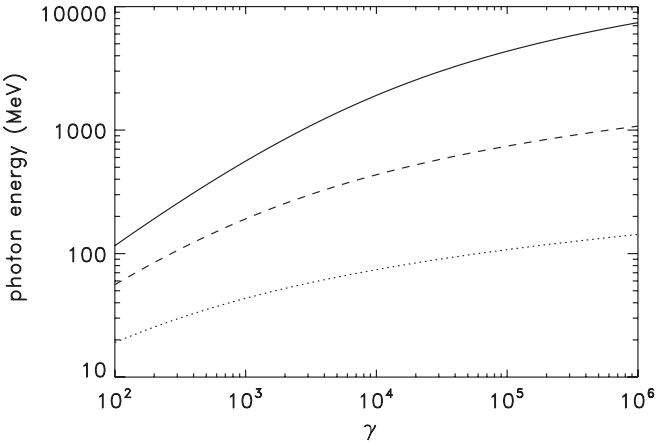

FIG. 4. Variation of the Compton component of heavy-ion bremsstrahlung with the Lorentz factor for bare lead ions penetrating a lead target. The solid curve shows the photon energy at which the cross section assumes the value 0.1 b. The dashed and dotted curves similarly correspond to fixed cross sections of 1 and 10 b.

Figure 5 shows the energy loss per unit path length, divided by the primary energy E and the atomic density N of the target, for bare lead ions penetrating a lead target. The radiative energy loss is generally given as

$$-\frac{dE}{dx} = N\int d\hbar\omega \frac{d\chi}{d\hbar\omega}. \tag{22}$$

Depletion of the main bremsstrahlung component due to electromagnetic dissociation of the projectile is at the level of 7%–9% at all energies displayed. Despite the decrease in the depletion factor $F(b)$ at a given impact parameter b (cf. Fig. 2), the reduction in the energy loss decreases slightly when γ is raised from 100 towards the LHC value of 3000. This is due to the increase in the impact-parameter range contributing to the main bremsstrahlung component. On the other hand, beyond the LHC energy where screening causes saturation in range, the reduction increases, albeit only slightly. For the energy loss due to the Compton component of the heavy-ion bremsstrahlung we apply the total cross section, (19), which includes the energy lost to both the emitted quantum and the electron recoiling as a result of the scattering of the virtual photon. At energies not much below the LHC energy, this component dominates the radiative energy loss (Fig. 5).

For heavy targets the energy loss per unit path length due to creation of electron-positron pairs is [13,20]

$$\left(-\frac{dE}{dx}\right)_{\rm PP} = \pi Z^2 Z_t^2 \alpha^2 r_e^2 N \gamma mc^2 \Lambda, \tag{23}$$

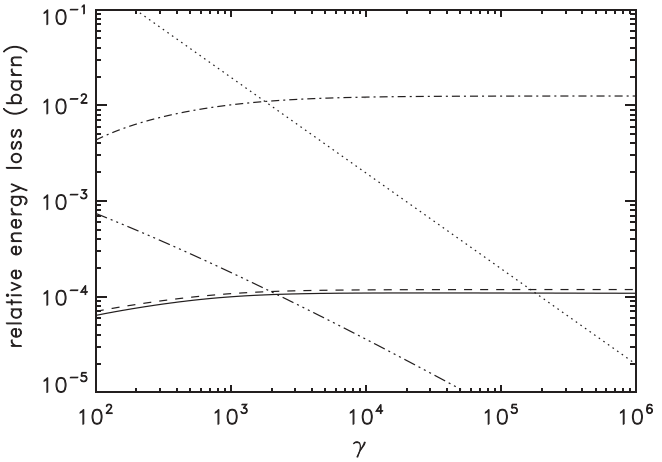

FIG. 5. Relative energy loss of a bare lead ion penetrating a lead target. The radiative loss due to the main bremsstrahlung component is shown, accounting for (solid curve) as well as ignoring (dashed curve) depletion due to electromagnetic dissociation. The triple-dot-dashed curve displays the Compton component of the radiative energy loss. The dotted curve shows the electronic energy loss, and the dot-dashed curve the energy loss due to electron-positron pair creation. To get the fractional energy loss $-E^{-1}dE/dx$ per centimeter, the ordinate should be multiplied by 3.30×10^{-2}.

where the logarithmic factor Λ is approximately given as

$$\Lambda = \frac{19}{9} \ln \frac{183 Z_t^{-1/3}}{1 + 4e^{11/6} 183 Z_t^{-1/3}/\gamma}. \tag{24}$$

The stopping power of the target due to atomic excitation and ionization, the "electronic energy loss," reads

$$\left(-\frac{dE}{dx}\right)_{\text{electr}} = \frac{4\pi Z^2 e^4}{m v^2} N Z_t L, \tag{25}$$

where $NZ_t = n$ is the average density of target electrons. In the quantum mechanical perturbation limit the "stopping number" L is given by Bethe's result including Fermi's density effect correction (see [21] or [22] for the explicit expression). For highly charged projectiles nonperturbative effects generally have to be included. At nonrelativistic energies they result in Bloch's correction, which bridges the gap from Bethe's result to Bohr's classical stopping formula. Reference [21] presents a treatment which includes all nonperturbative corrections as well as the effect of the finite size of the projectile nucleus at any energy in one single calculation. For energies sufficiently high that the density effect is in full action and close collisions are limited by the finite size of the projectile nucleus, the logarithmic factor L takes the remarkably simple form

$$L \rightarrow \ln(1.62 c/R\omega_{\text{pl}}), \tag{26}$$

where $\omega_{\text{pl}} = \sqrt{4\pi n e^2/m}$ is the plasma frequency of the target. For heavy projectiles in condensed matter Eq. (26) applies quite accurately for γ values beyond 100.

As is clear from Fig. 5 the energy loss of a heavy bare ion is dominated by electronic excitation and ionization of target atoms at low and moderate values of γ and by pair production at high γ. The sum of these two components will provide the energy loss to about 1% at all energies, bremsstrahlung processes contribute insignificantly. With all components scaling approximately with Z^2, that is, in approximately the same manner, this conclusion is independent of the projectile charge. Note that the reading for the Compton contribution for our standard case is 5.45×10^{-4} b, which translates to a correction to the stopping number of $\Delta L = 0.064$, which is within the error bars of the experiment discussed at the end of Sec. II B3.

III. HEAVY-ION BREMSSTRAHLUNG IN AXIALLY ALIGNED CRYSTALS

When a relativistic heavy ion moves through a single crystal near a low-index axial direction and passes relatively close to a row of atoms, deflecting slightly in each encounter, correlation between successive scattering events implies that the ion's trajectory effectively is the same as that resulting from interaction with a continuum row obtained by smearing the target charges along the direction of the axis [23–25]. With V denoting the ion-atom interaction potential energy and z the coordinate along the atomic row, the corresponding continuum potential reads

$$U(r) = \frac{1}{d} \int_{-\infty}^{\infty} dz V(r,z), \tag{27}$$

where r is the transverse distance to the center of the string and d the average spacing between atoms along it. For a single isolated row of atoms U has rotational symmetry, Eq. (27). For a true crystal there will be a periodicity in transverse space, $U = U(\mathbf{r})$. For motion close to a low-index planar direction a similar continuum approximation applies.

For a particle governed by the continuum potential, the z component of the force exerted by the crystal vanishes. Hence the longitudinal momentum p_z will be a constant of motion. In consequence, also the "longitudinal energy" $E_z \equiv (p_z^2 c^2 + M^2 c^4)^{1/2}$ as well as its "transverse" counterpart $E_\perp \equiv E - E_z$ will be conserved. For motion at a small angle ψ to the atomic row, the transverse energy takes the form

$$E_\perp = \frac{p_\perp^2}{2\gamma M} + U(r) = \frac{1}{2} p v \psi^2 + U(r), \tag{28}$$

where $p_\perp$ is the component of the projectile momentum $\mathbf{p}$ transverse to the string. While moving through the crystal the transverse position and momentum, r and $p_\perp$, change as transverse kinetic energy [first quantity on the right-hand side of Eq. (28)] is traded for potential energy, and vice versa. Also the angle changes. Typical values for ψ for motion governed by the continuum potential may be estimated by equating $\frac{1}{2} p v \psi^2$ to the height of the potential, $U(0)$. For any reasonable choice of potential the result approximates Lindhard's critical angle ψ_1, defined as

$$\psi_1 = \left(\frac{4 Z Z_t e^2}{p v d}\right)^{1/2}. \tag{29}$$

Motion at transverse energies up to, roughly, the height of the continuum potential is also known as channeling. See Refs. [23–25] for further details.

Governing of the projectile motion by highly correlated deflections in a single crystal influences the emission of bremsstrahlung in two ways. The gradually bending

trajectories, whose projections in transverse space generally are far from straight lines and determined by conservation of transverse energy, and approximate conservation of angular momentum in the interaction with each string (if projectiles come sufficiently close), give rise to the emission of so-called channeling radiation. The focusing of the positively charged projectiles in parts of transverse space far from strings, on the other hand, gives rise to a weakening of the emitted bremsstrahlung compared to that due to interactions with individual atoms in a similar but amorphous target. For heavy projectiles channeling radiation, where the coherence in scattering on target atoms is carried on to the radiation, is generally confined to energies much lower than those discussed in the previous section (cf. [3]). It is therefore not considered further. By far, the main effect of the coherence in scattering on heavy-particle bremsstrahlung is the creation of a nonuniform particle flux which leads to depletion of the bremsstrahlung, including a nearly complete extinction of the main component, for perfect alignment between the direction of incidence and the crystal axis.

In this paper we consider solely axial alignment and generally focus on interaction with just a single isolated string of atoms at any given time. For applications we need an explicit expression for the continuum potential. A convenient candidate is the so-called Doyle-Turner potential, which is based on an analytical approximation to relativistic Hartree-Fock atomic potentials,

$$U(r) = \frac{Ze^2}{a_0}\frac{2a_0^2}{d}\sum_{i=1}^{4}\frac{a_i}{C_i}e^{-r^2/C_i}, \tag{30}$$

where

$$C_i = C_i(\rho) \equiv b_i/4\pi^2 + \rho^2 \tag{31}$$

and ρ denotes the two-dimensional root-mean-square thermal displacement of the atom from the equilibrium position [cf. Eq. (39)]. For details and explicit values of the coefficients a_i (Å) and b_i (Å^2), see Ref. [26] or Refs. [24,27]; for values of the thermal vibration amplitude, see [28]. The Doyle-Turner potential is quite accurate when thermally averaged as in Eqs. (30) and (31) [27].

A. Reaction yields for channeled particles

In order to determine the variation of the bremsstrahlung yield with the degree of alignment we proceed as described in, for instance, Ref. [24]. A key point is a rapid trend towards statistical equilibrium, which implies that calculation of individual projectile trajectories and subsequent averaging may be avoided [23].

A projectile incident at the crystal at an angle $\psi_{\rm in}$ to the considered axial direction enters the crystal with a transverse kinetic energy of $\frac{1}{2}pv\psi_{\rm in}^2$. Entrance at transverse position $\mathbf{r}_{\rm in}$ further gives it a potential energy $U(\mathbf{r}_{\rm in})$ whereby its transverse energy (just inside the crystal surface) assumes the value

$$E_\perp = \tfrac{1}{2}pv\psi_{\rm in}^2 + U(\mathbf{r}_{\rm in}) = 2ZZ_te^2d^{-1}\,(\psi_{\rm in}/\psi_1)^2 + U(\mathbf{r}_{\rm in}), \tag{32}$$

where Lindhard's critical angle ψ_1 is defined by Eq. (29). The distribution of the incident beam over $(\mathbf{r}_{\rm in},\psi_{\rm in})$ determines the $E_\perp$ distribution. The distribution over $\mathbf{r}_{\rm in}$ is obviously uniform on the atomic scale upon entrance. For a given $\psi_{\rm in}$ the distribution in transverse energy right inside the crystal surface hence is

$$g(E_\perp,\psi_{\rm in}) = \frac{1}{A_0}\int_{A_0} d^2r_{\rm in}\,\delta\!\left(E_\perp - \frac{1}{2}pv\psi_{\rm in}^2 - U(\mathbf{r}_{\rm in})\right), \tag{33}$$

where the transverse area per string is related to the atomic density of the target N and the longitudinal atomic spacing d as $A_0 \equiv \pi r_0^2 = (Nd)^{-1}$. Since the continuum potential is flat over large regions between strings, the $E_\perp$ distribution peaks around $\frac{1}{2}pv\psi_{\rm in}^2$ for positively charged projectiles.

Let $\Pi_{\rm in}$ denote the probability that a projectile with transverse energy $E_\perp$ takes part in the process of interest. The reaction yield is then determined by integration of the product $g\Pi_{\rm in}$ over transverse energy. Below we neglect "dechanneling," that is, we ignore the possibility that the distribution g may change with penetrated depth. With g determined by surface transmission, Eq. (33), the directional dependence of the reaction yield of the process reads

$$X(\psi_{\rm in}) = \frac{2}{r_0^2}\int_0^{r_0} dr\, r\,\Pi_{\rm in}\!\left(\frac{1}{2}pv\psi_{\rm in}^2 + U(\mathbf{r})\right). \tag{34}$$

Note that in accord with Eq. (32), X actually depends only on the ratio $\psi_{\rm in}/\psi_1$. If the reaction process is characterized by an impact-parameter-dependent probability P_X, the collision partners may be treated as moving on well-localized paths according to classical mechanics, and interaction between collision partners located in different channels is rare, we may express the function $\Pi_{\rm in}$ as

$$\Pi_{\rm in}(E_\perp) = A_0\int d^2r'\int d^2r\; P_t(\mathbf{r}')P(E_\perp;\mathbf{r})P_X(\mathbf{r}-\mathbf{r}'), \tag{35}$$

where both integrals extend over the single-string area A_0. The probability distributions P and P_t for the projectile and target object in transverse space are normalized inside this area. Provided that also the reaction probability is normalized and that, to good approximation, $\int d^2r\; P_X(\mathbf{r}-\mathbf{r}') = 1$ for all $\mathbf{r}'$, where $P_t(\mathbf{r}')$ is appreciable, $\Pi_{\rm in} = 1$ and hence $X = 1$ for $\psi_{\rm in}$ well beyond ψ_1 ("random" incidence), which produces a uniform probability, $P = 1/A_0$. For a completely localized interaction, $P_X(\mathbf{r}-\mathbf{r}') = \delta(\mathbf{r}-\mathbf{r}')$, Eq. (35) reduces to

$$\Pi_{\rm in}(E_\perp) = A_0\int d^2r\, P_t(\mathbf{r})P(E_\perp;\mathbf{r}). \tag{36}$$

For an axially channeled beam of particles initially centered around a given transverse momentum, there will be a trend towards statistical equilibrium in transverse phase space [23]. Equal probability in the allowed region of transverse phase space in turn leads to equal probability $P(E_\perp;\mathbf{r})$ of finding a particle of given $E_\perp$ anywhere inside the accessible area in direct space. Hence

$$P(E_\perp;\mathbf{r}) = \frac{1}{A(E_\perp)}\Theta(E_\perp - U(\mathbf{r})), \tag{37}$$

where $\Theta(x)$ is the Heaviside function. The accessible area is given as $A(E_\perp) = A_0 - \pi r_\downarrow^2$, where $r_\downarrow$ is the minimum distance of approach to the string classically, that is, $E_\perp = U(r_\downarrow)$ for $E_\perp < U(0)$. With distribution (37) the probability

$\Pi_{\rm in}$ of a completely localized interaction, Eq. (36), reduces further to

$$\Pi_{\rm in}(E_\perp) = \frac{A_0}{A(E_\perp)} \int_{r_\downarrow(E_\perp)}^{r_0} dr 2\pi r P_t(r) \tag{38}$$

in the single-string approximation.

B. Interaction with target nuclei

If the target object is a nucleus at a lattice site, its distribution function P_t assumes the form

$$P_t(\mathbf{r}') = (\pi\rho^2)^{-1} \exp(-r'^2/\rho^2) \tag{39}$$

within the harmonic approximation for interatomic forces with the equilibrium position at the center of the channel. Insertion of this result along with Eq. (37), corresponding to statistical equilibrium, simplifies (35) to

$$\Pi_{\rm in}(E_\perp) = \frac{A_0}{A(E_\perp)} \frac{1}{\pi\rho^2} \int d^2r' \int_{A(E_\perp)} d^2r\, e^{-r'^2/\rho^2} P_X(\mathbf{r}-\mathbf{r}'). \tag{40}$$

For processes of a very short range, that is, shorter than all other characteristic lengths in the problem, the reaction probability may be approximated by a δ function. With $\rho \ll r_0$ the corresponding expression, (38), reduces to

$$\Pi_{\rm in}(E_\perp) = \frac{A_0}{A(E_\perp)} e^{-(r_\downarrow(E_\perp)/\rho)^2}. \tag{41}$$

For random incidence this reduces to 1 since in this case $A(E_\perp) = A_0$ and $r_\downarrow(E_\perp) = 0$. If we insert expression (41) in Eq. (34) for $\psi_{\rm in} = 0$, we obtain a minimum yield of

$$X_{\rm min} = X(0) = \frac{\rho^2}{r_0^2} = \pi N d \rho^2, \tag{42}$$

still observing $\rho \ll r_0$.

Since P_X in expression (40) for $\Pi_{\rm in}$ is a function of the relative coordinate $\mathbf{r}'' \equiv \mathbf{r}' - \mathbf{r}$, it is convenient to change the outer integration variable from the target coordinate $\mathbf{r}'$ to $\mathbf{r}''$. We confine our attention to cases where P_X depends solely on the magnitude of $\mathbf{r}''$ and not the direction whereby one angular integration is trivial. With ϕ'' denoting the angle between the relative and the projectile coordinate, we have $r'^2 = r^2 + r''^2 + 2rr''\cos\phi''$. Interchanging the order of integration, we may then rewrite Eq. (40) as

$$\Pi_{\rm in}(E_\perp) = \frac{A_0}{A(E_\perp)} \frac{2}{\rho^2} \int_{r_\downarrow(E_\perp)}^{r_0} dr\, r\, e^{-r^2/\rho^2} \int_0^\infty dr'' r'' e^{-r''^2/\rho^2} \times P_X(r'') \int_0^{2\pi} d\phi'' e^{-2rr''\cos\phi''/\rho^2}. \tag{43}$$

Extension of the integration over the relative coordinate to all of transverse space is obviously an approximation since both $\mathbf{r}$ and $\mathbf{r}'$ are confined to the single-string area. However, for processes with effective ranges much less than r_0 and a target density highly concentrated near the string, the approximation is quite accurate (cf. the discussion above). The change of coordinates formally leads to an upper limit for r'' of $r_0 + r$ and, for $r'' > r_0 - r$, to exclusion of angles with $\cos\phi'' > (r_0^2 - (r^2 + r''^2))/2rr''$. Including the full range of angles, the integral over ϕ'' may be performed analytically. The result is expressed in terms of the modified Bessel function I_0 [29] such that

$$\Pi_{\rm in}(E_\perp) = \frac{4\pi A_0}{A(E_\perp)} \rho^2 \int_{r_\downarrow(E_\perp)/\rho}^{r_0/\rho} dy\, y\, e^{-y^2} \times \int_0^\infty dx\, x\, e^{-x^2} I_0(2xy) P_X(x\rho), \tag{44}$$

where we have introduced the variables $x = r''/\rho$ and $y = r/\rho$.

C. Interaction with target electrons

To obtain $\Pi_{\rm in}$ for a process involving target electrons the probability $P_t(\mathbf{r}')$ appearing in Eq. (35) has to reflect their density in transverse space $n_e^{(2D)}$. Generally, the charge density in the continuum model may be obtained by applying the Poisson equation to the thermally averaged continuum potential, the corresponding charge density in two-dimensional transverse space results upon further multiplication by d. Subtraction of the nuclear charge density $Z_t e(\pi\rho^2)^{-1}\exp(-r'^2/\rho^2)$ and division of the result by the electron charge $-e$ produces the requested two-dimensional electron number density. The normalized probability P_t is obtained by finally dividing by the total number of electrons per atom. For the thermally averaged Doyle-Turner potential, (30), this procedure results in a slight unphysical modulation. Instead, the probability may be obtained from Doyle and Turner's fit to the x-ray scattering factor [26], which directly reflects the electron density. In the continuum approximation and including the smearing due to thermal vibrations, the result is

$$P_t(r') = \frac{1}{Z_t} n_e^{(2D)}(r') = \frac{1}{Z_t}\left[\frac{c^{(X)}}{\pi\rho^2} e^{-r'^2/\rho^2} + \frac{1}{\pi}\sum_{i=1}^4 \frac{a_i^{(X)}}{C_i^{(X)}} e^{-r'^2/C_i^{(X)}}\right], \tag{45}$$

where

$$C_i^{(X)} = C_i^{(X)}(\rho) \equiv b_i^{(X)}/4\pi^2 + \rho^2 \equiv \rho^2 D_i^{(X)}(\rho). \tag{46}$$

For details and explicit values of the coefficients $c^{(X)}$, $a_i^{(X)}$, and $b_i^{(X)}$ see [26]; $D_i^{(X)}$ is introduced for later convenience. Note that $c^{(X)} + \sum_{i=1}^4 a_i^{(X)} = Z_t$. Figure 6 displays the probability, (45), of a silicon crystal aligned along the strongest axis together with the corresponding probability obtained from the potential, (30), and the more localized nuclear density, (39). The probabilities are plotted out to the single-string radius r_0. The nuclear probability effectively vanishes long before this limit. The electronic probability, on the other hand, is much broader and is not completely diluted at r_0.

The probability, (45), is normalized in the entire transverse space. For use in expression (35) for $\Pi_{\rm in}$ a probability normalized to the single-string area ($r < r_0$) is needed. We acquire this simply by multiplying expression (45) by a proper constant,

$$C_N = 1/\int_{A_0} d^2r'\, P_t(r') = 1/\left[1 - \frac{1}{Z_t}\sum_{i=1}^4 a_i^{(X)} e^{-r_0^2/C_i^{(X)}}\right], \tag{47}$$

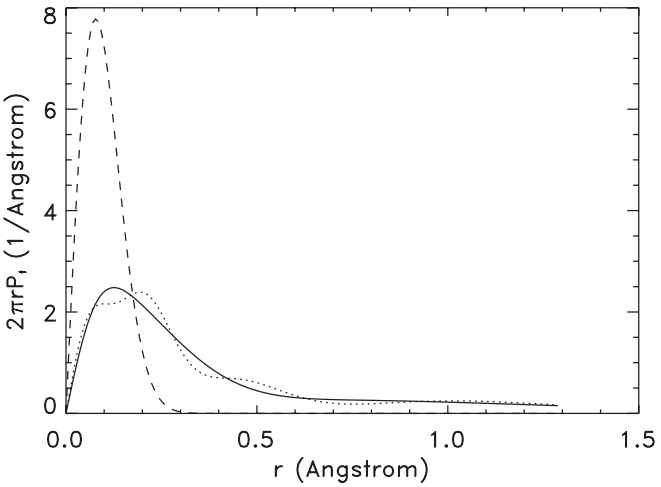

FIG. 6. Target object probability $2\pi r P_t$ as a function of transverse distance r for a silicon single crystal aligned along the ⟨110⟩ direction. The solid curve corresponds to the electron probability, (45); the dotted curve, to the electron probability obtained from the thermally averaged Doyle-Turner potential, (30); and the dashed curve, to the probability distribution, (39), for target nuclei. The crystal temperature is 300 K.

where we have assumed $\rho \ll r_0$ in the last step. Since not all of the quantities $C_i^{(X)}$ are small compared to r_0^2 the denominator is less than 1, whereby the normalization factor ends up being somewhat larger than 1. For the example shown in Fig. 6, the density reconstructed from the fit by Doyle and Turner produces a total of 12.89 electrons inside the single-string radius r_0. Accordingly, in this case we multiply the probability, (45), by the constant $C_N = 14/12.89$. Obviously, more sophisticated choices could be made, for instance, choices which reflect that the missing density primarily pertains to larger distances. However, if we were to account for this, the lack of axial symmetry should also be accounted for. Since the correction is moderate we have decided on the simple renormalization with a constant factor, C_N of Eq. (47).

In statistical equilibrium, Eq. (37), $\Pi_{\rm in}$ is given by Eq. (40) with replacement of $(\pi\rho^2)^{-1}\exp(-r'^2/\rho^2)$ by expression (45) for processes involving target electrons. For processes of range shorter than all other characteristic lengths in the problem, the reaction probability may be approximated by a δ function. Again, with $\rho \ll r_0$ the yield of such close-encounter processes involving electrons reduces, by inclusion of the normalization factor C_N, to

$$\Pi_{\rm in}(E_\perp) = \frac{A_0}{A(E_\perp)}\frac{C_N}{Z_t}\left[c^{(X)}e^{-(r_\downarrow(E_\perp)/\rho)^2} + \sum_{i=1}^{4} a_i^{(X)}\left\{e^{-(r_\downarrow(E_\perp))^2/C_i^{(X)}} - e^{-r_0^2/C_i^{(X)}}\right\}\right]. \quad (48)$$

For $E_\perp = U(0)$, corresponding to $r_\downarrow = 0$, the right-hand side of Eq. (48) reduces further, by application of Eq. (47), to 1 as required.

In the general case we may proceed as described in the previous subsection for interactions with target nuclei. Including the normalization factor C_N and performing the angular integrations as for interactions with nuclei, $\Pi_{\rm in}$ is obtained from Eq. (44) by the following substitution:

$$I_0(2xy)e^{-x^2-y^2} \to \left[c^{(X)}I_0(2xy)e^{-x^2-y^2} + \sum_{i=1}^{4}\frac{a_i^{(X)}}{D_i^{(X)}} \times I_0\left(2xy/D_i^{(X)}\right)e^{-(x^2+y^2)/D_i^{(X)}}\right]\frac{C_N}{Z_t}. \quad (49)$$

To obtain Eq. (49) we have again extended the integration over the relative coordinate over all of transverse space. This approximation is less accurate for processes involving target electrons than target nuclei since the electron density is not completely diluted near the edge of the single-string area. However, this is of little concern here since (a) the electron component due to scattering of virtual photons of target particles on the projectile is a small correction to the main contribution and (b) the upper end of the Compton component is essentially due to completely localized encounters. Even for the lower part of the latter component the error committed will be moderate since the fraction of the electrons placed near the edge is quite small.

D. Results

The variation in the spectrum of the main bremsstrahlung component with the angle of incidence to a major crystallographic direction is particularly simple in the limit of complete screening: In this limit, by definition, the second term in the square root in Eq. (3) dominates at all frequencies where the cross section multiplying the virtual photon intensity has support, whereby the dependence of the radiation cross section on energy and impact parameter separates; that is,

$$\frac{d^3\chi}{d\hbar\omega d^2b} = \frac{d\chi}{d\hbar\omega}S(b). \quad (50)$$

Here $d\chi/d\hbar\omega$ is the usual radiation spectrum obtained after integration over b for the case with no depletion (due to electromagnetic dissociation or something similar), and the impact-parameter dependence is given as

$$S(b) = \frac{1}{2\pi\ln(Ca_{\rm TF}/R_\Sigma)}\frac{1}{b^2}\left[\frac{b}{a_{\rm TF}}K_1\left(\frac{b}{a_{\rm TF}}\right)\right]^2. \quad (51)$$

A depletion factor $F(b)$ may be included on the right-hand side of Eq. (50) if need be. The separation, (50), implies that, in the limit of complete screening, the variation in the main bremsstrahlung component with the degree of alignment (that is, angle) is the same throughout the spectrum, at any frequency determined by the factor $S(b)$, Eq. (51). The same conclusion holds for the bremsstrahlung component due to scattering of virtual photons of target electrons on the projectile—albeit with R_Σ in Eq. (51) replaced by the radius R of the projectile (cf. Sec. II B2).

Our standard case in the examples in this section is bare lead ions incident on a silicon single crystal near the strongest axis, that is, the ⟨110⟩ axis. The crystal is cooled to 100 K and we assume the primary energy sufficiently high that screening is complete; in praxis this requires LHC energies ($\gamma = 3000$) and beyond (see discussion in Sec. II C). Comments on lower energies are included.

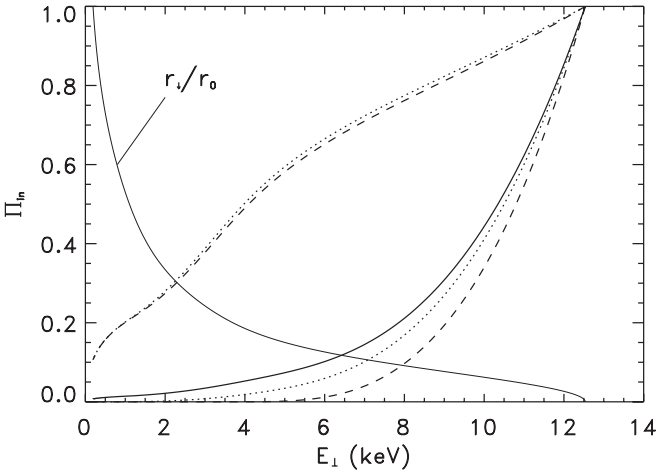

FIG. 7. Probability Π_{in} for bremsstrahlung emission for a bare lead ion penetrating a silicon crystal near the ⟨110⟩ axis as a function of transverse energy in the limit of complete screening. The crystal is cooled to 100 K, and only a single string is considered. Dotted curves show the variation of the main bremsstrahlung component (lower curve) and the component due to scattering of virtual photons of target electrons on the projectile (upper). The solid curve is the sum of the dotted curves weighted according to the total cross sections. Dashed curves pertain to truly close encounters between target object and projectile nucleus, that is, a δ-function interaction; the lower curve is for interaction with target nuclei, and the upper for interaction with target electrons. For reference, the figure also displays the variation of the minimum distance of approach relative to the single-string radius (curve decreasing with increasing transverse energy).

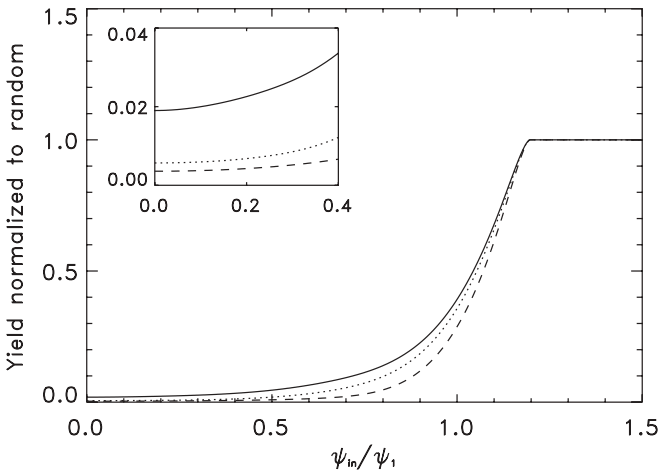

FIG. 8. Channeling yields corresponding to Fig. 7. Inset: The variation near the minimum. The electron contribution is not shown separately; otherwise, the curves are as in Fig. 7.

Figure 7 displays the probability Π_{in} for our standard case calculated in the single-string approximation as described in previous subsections. The transverse energy varies from a minimum of 0.19 keV, the potential energy at the single-string radius r_0, to a maximum of 12.53 keV, the potential energy at the position of the atomic string ($r = 0$). The two lowest curves correspond to the main bremsstrahlung component (dotted curve) and contact collisions between projectile and target nuclei (dashed curve). Obviously the former is not much different from the latter, revealing that, on the channeling scale, bremsstrahlung is essentially a close-encounter process. Complete screening represents the ultimate and longest effective range of the process. At lower energies, where screening is not complete, the probability Π_{in} for the main bremsstrahlung component will fall between the two curves, that is, it will be even closer to the yield of a truly close-encounter process than the dotted curve in Fig. 7. Furthermore, the position will depend on the photon energy; at lower photon energies it will be closer to the upper curve, and at higher photon energies it will be closer to the lower curve. The uppermost curve in Fig. 7 displays the variation with transverse energy of the probability Π_{in} for the bremsstrahlung component which is due to scattering of the virtual photons of target electrons on the projectile. It is very close to the curve that results for a δ-function interaction between target electrons and projectile nucleus. The structures in the electron curves reflect the changes in falloff of the electron probability with increasing distance visible in Fig. 6. Since electrons are distributed much more widely than target nuclei in the channel, damping at low transverse energies, where the projectile is restricted to move at relatively large distances from (the center of) the atomic row, is not nearly as dramatic for the electron as for the main component. However, since the total cross section for the electron component (at random incidence) is only about $1/Z_t$ that of the main component, the weighted sum of the two Π_{in} functions is dominated by the main bremsstrahlung component except for a lift from essentially 0 at the lowest transverse energies.

Figure 8 shows the variation with angle of incidence to the ⟨110⟩ axis of the main bremsstrahlung component as well as the weighted sum of this and the electron component for our standard case. The probabilities in Fig. 7 were used as input. Since screening is assumed to be complete, the variation is the same at all photon frequencies. The yield of the main bremsstrahlung component is not much different from that of a true close-encounter process. However, the electron contribution adds to the difference, in particular, to the minimum yield obtained at parallel incidence: Including the electron contribution, the minimum yield is about 5 times higher than that pertaining to contact collisions with target nuclei.

Variation in the target temperature leads to change in the distribution of target atoms. Since vibration amplitudes are short compared to the atomic radius, such variation primarily influences the main bremsstrahlung component. Figure 9 shows how the weighted sum of the yield of the main and the electron contribution changes for our standard case when the crystal temperature is raised from 100 to 300 K. The increase in the minimum yield as well as the narrowing of the dip closely reflects the change that would appear for contact collisions.

Figure 10 shows the variation with angle of incidence of the upper end of the Compton component of the bremsstrahlung spectrum for the same collision system as in Figs. 7 and 8. The high-energy end pertains to very close collisions, and hence the variation reflects a probability Π_{in} essentially identical to the upper dashed curve in Fig. 7. Since the Compton component stands out clearly at low photon energies, so will its variation with angle of incidence, which obviously is less dramatic than that of the sum of the components due to scattering of virtual photons of target constituents off the

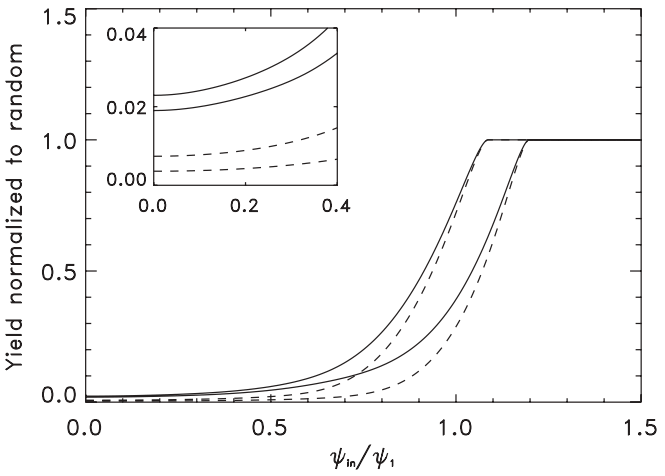

FIG. 9. As Fig. 8, but including results for $T = 300$ K (upper curves).

projectile. Note that the variation of the Compton component displayed in Fig. 4 in Ref. [3] was based on a considerably rougher calculation than presented here.

As commented in Sec. II C, radiation emitted by electrons and positrons resulting from pair-production events falls in the same energy range as the Compton component of the heavy-ion bremsstrahlung. Besides the different dependence on target thickness, the variation with angle of incidence is also different: even at LHC energies pair creation is reduced by a factor of as much as 40 for lead ions incident on a cooled silicon crystal parallel to the ⟨110⟩ axis (see also Sec. IV).

In our last example we lower the energy of the ^{208}Pb projectile to the value corresponding to $\gamma = 170$ which was used as the standard in Sec. II C. In that case screening is of little importance: according to Eq. (3) the effective range of the interaction is determined by the screening length for $\omega'/\gamma c < 1/a$, which, with the Thomas-Fermi length for silicon used for a, implies photon energies below 1.7 MeV, that is, photon energies way below the position of the GDR peak of ^{208}Pb. Furthermore, the effective range of the interaction is short: since the modified Bessel functions $K_n(x)$ fall off

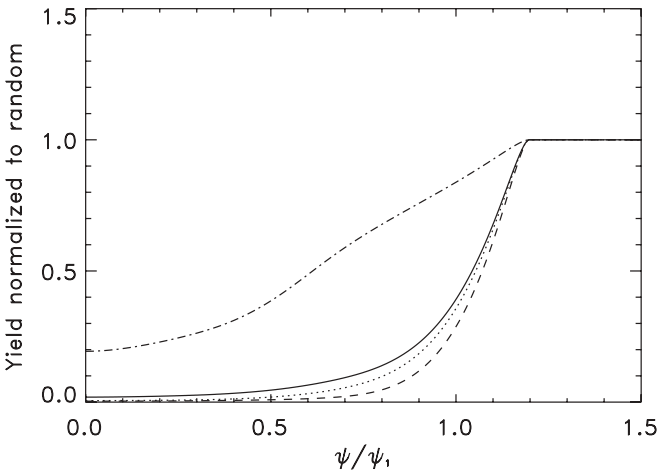

FIG. 10. As Fig. 8, but including the Compton component (dot-dashed curve).

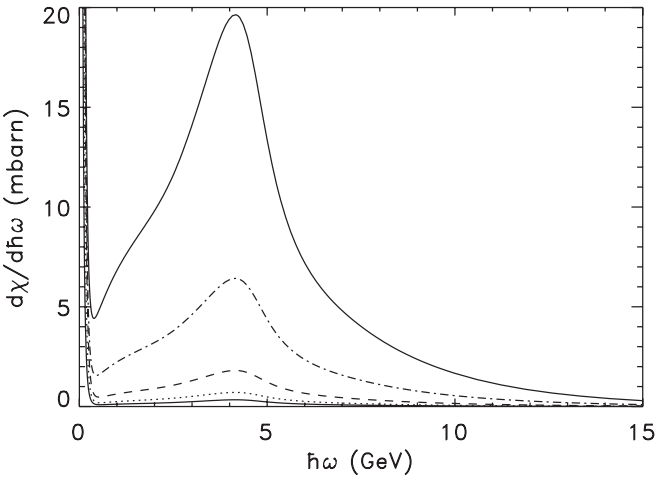

FIG. 11. Total bremsstrahlung spectrum for bare lead ions penetrating a silicon single crystal near the ⟨110⟩ axis at $\gamma = 170$. Spectral values increase with angle of incidence; plots are shown for $\psi/\psi_1 = 0$ (parallel incidence; lower solid curve), 0.5 (dotted curve), 0.8 (dashed curve), 1.0 (dot-dashed curve), 2.0 (upper solid curve; spectrum as for random placement of crystal atoms). The crystal is cooled to 100 K.

exponentially for $x > 1$, the range may be estimated as $\gamma c/\omega'$ according to Eq. (2), which, upon substitution of the GDR-peak energy for $\hbar\omega'$, amounts to 0.025 Å. Since this is just about one-third of the two-dimensional thermal vibration amplitude ρ for silicon at 100 K, the bremsstrahlung processes corresponding to scattering of virtual photons of target objects on the projectile may be considered of zero range in channeling contexts. We may argue along the same lines for the Compton component: for photon energies above 4.4 MeV, the effective range of the interaction is less than ρ at 100 K; that is, for such energies this interaction also may be considered of zero range in channeling contexts.

Figure 11 shows the variation with angle of incidence of the bremsstrahlung spectrum for ^{208}Pb projectiles penetrating a silicon single crystal at $\gamma = 170$. The spectrum includes the main component, the Compton component, and the component due to scattering of virtual photons of target electrons on the projectile. For the latter we have set the value at large angles, corresponding to the incidence on a random arrangement of silicon atoms, to $1/12.94$ times the main component under the same conditions; the deviation from $1/Z_t$ accounts for the difference in logarithm (8) for the two processes, due to different minimum impact parameters, at the GDR-peak energy. To obtain the spectral variation with angle we apply the variations for δ-function interaction; this corresponds to multiplying the main component (for random target) by the values represented by the dashed curve in Fig. 10 and the electron components (for random target) by the values represented by the dot-dashed curve in the same figure. Figure 11 displays the total bremsstrahlung spectrum for five angles of incidence to the ⟨110⟩ axis, ranging from parallel incidence to incidence at an angle sufficiently large that the spectrum for a random target obtains. The variation is dramatic.

The logarithmic plot in Fig. 12, which repeats the data in Fig. 11, clearly shows the variation of the Compton component along with that of the other two components. As revealed

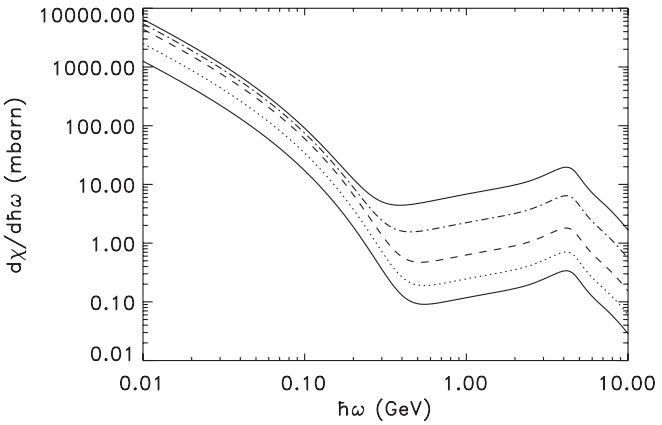

FIG. 12. A log-log plot of the spectra in Fig. 11.

in the figure, the variation below, roughly, γ MeV, where bremsstrahlung mainly is due to the Compton process, is much less dramatic than the variation of the spectrum around the peak at, roughly, 25γ MeV. The difference is particularly clear for the upper three curves. Note, also, that due to the different scaling of the various components with Z_t, the Compton component is relatively larger for a silicon than a lead target (Fig. 3).

IV. CONCLUDING REMARKS: PAIR PRODUCTION

Let us conclude with some remarks on electron-positron pair creation, which determines the energy loss for bare heavy ions penetrating matter at sufficiently high energies as discussed above. There are two major components which contribute about equally to the energy loss: (a) one is due to conversion of virtual photons of the projectile in the field of target atoms; (b) the other, to conversion of virtual photons of target atoms in the field of the projectile. The latter component (b) contains a limitation in range since the source of the virtual photons is a neutral atom; that is, the virtual photon spectrum is depleted rapidly for impact parameters larger than the screening radius of the target atom. The former component (a) involves the standard Bethe-Heitler cross section, whose range also is limited by atomic screening deriving from electron scattering in the perturbing field *viz* the field of the target atom. Hence the screening radius appears in the yield of this component as well, but the source of virtual photons is unscreened; that is, the impact parameter between projectile and target atom is not limited by screening. This implies that only component (b) is guaranteed to display a close-encounter behavior similar to that shown in Figs. 8 and 9 for bremsstrahlung.

While the above observation is generally true, the effective range of component (a) does not exceed the screening radius at moderate γ as that in our standard case in Sec. II C since the minimum requirement on the photon energy is high on the atomic scale ($2mc^2$). Hence at $\gamma = 170$ very pronounced channeling dips appear in the energy loss of a heavy ion to electron-positron pairs. The same still holds true at LHC energies. For a lead ion with $\gamma = 3000$ penetrating a silicon crystal cooled to 100 K the minimum yield of the total number of pairs produced by process (a) upon alignment with the $\langle 110 \rangle$ axis is as low as 0.014, that is, 1.4% of the value for random impact (0.025 if interaction with individual electrons is included). This implies that the effective maximum impact parameter is of the order of the screening radius. In turn, this means that the effective minimum virtual photon energy is considerably above the threshold, which reflects the slow rise from 0 of the cross section for photon conversion to electron-positron pairs (cf. Ref. [8]).

The energy loss to atomic excitation and ionization shows only limited variation with angle of incidence to a major crystallographic axis, in particular, at high energies. Since it derives from interaction with target electrons, dips in yield cannot be more pronounced than that for the high-energy end of the Compton component of bremsstrahlung (cf. Fig. 10). Furthermore, at high energies the effective range of the interaction is much wider than the crystal channel as revealed by the logarithm, (26), whose argument is the ratio of the maximum to the minimum lengths effective in the interaction. Only about half of the logarithm pertains to collisions with impact parameters smaller than the screening radius. Altogether we may expect the electronic energy loss to vary by not more than roughly a factor of 2 when tilting the crystal. For lead ions incident at large angles to major crystallographic directions of a silicon single crystal, which corresponds to the incidence on an amorphous silicon target, energy loss to electron-positron pairs is larger than that to atomic excitation and ionization for γ values beyond 9×10^3 [13,20]. For such high γ values we may expect pronounced dips in energy loss upon alignment with a crystal axis. The depletion deepens with increasing energy at first as the electronic energy loss gradually becomes insignificant but is expected to weaken again later as the effective range of pair-creation component (a) grows well beyond the screening length.

ACKNOWLEDGMENTS

We thank Ulrik Uggerhøj for his interest in the project and for critical reading of the manuscript. This work was supported by the Danish Natural Science Research Council.

[1] A. H. Sørensen, Phys. Rev. A **81**, 022901 (2010).
[2] S. J. Brodsky, F. Fleuret, C. Hadjidakis, and J. P. Lansberg, arXiv:1202.6585 [hep-ph] (2012).
[3] A. H. Sørensen and T. V. Jensen, Nuovo Cimento C **34**(4), 19 (2011).
[4] J. D. Jackson, *Classical Electrodynamics* (Wiley, New York, 1975).
[5] J. C. Baggesen and A. H. Sørensen, Nucl. Instr. Meth. B **267**, 2662 (2009).
[6] A. J. Baltz, G. Baur, D. d'Enterria, L. Frankfurt, F. Gelis, V. Guzey, K. Hencken, Yu. Kharlov, M. Klasen, S. R. Klein, V. Nikulin, J. Nystrand, I. A. Pshenichnov, S. Sadovsky, E. Scapparone, J. Seger, M. Strikman, M. Tverskoy, R. Vogt, S. N. White, U. A. Wiedemann, P. Yepes, and M. Zhalov, Phys. Rep. **458**, 1 (2008); see Chap. 7.
[7] J. J. Gaardhøje, Annu. Rev. Nucl. Part. Sci. **42**, 483 (1992).
[8] W. Heitler, *The Quantum Theory of Radiation* (Oxford University Press, London, 1954) (reprinted by Dover, New York, 1984).

[9] V. Z. Jankus, Phys. Rev. **90**, 4 (1953).
[10] J. Schwinger, Phys. Rev. **75**, 898 (1949).
[11] L. I. Schiff, Phys. Rev. **87**, 750 (1952).
[12] S. Datz, H. F. Krause, C. R. Vane, H. Knudsen, P. Grafström, and R. H. Schuch, Phys. Rev. Lett. **77**, 2925 (1996).
[13] A. H. Sørensen, AIP Conf. Proc. **680**, 102 (2003).
[14] A. Belkacem and A. H. Sørensen, Rad. Phys. Chem. **75**, 656 (2006).
[15] G. Molière, Z. Naturforsch. **2a**, 133 (1947) (in German).
[16] P. B. Eby, Phys. Rev. A **43**, 2258 (1991).
[17] C. R. Vane, S. Datz, E. F. Deveney, P. F. Dittner, H. F. Krause, R. Schuch, H. Gao, and R. Hutton, Phys. Rev. A **56**, 3682 (1997).
[18] K. Hencken, D. Trautmann, and G. Baur, Phys. Rev. C **60**, 034901 (1999).
[19] An estimate of the ratio of the two contributions is given in Ref. [1]. Since the results in Ref. [18] pertain to the center-of-mass system of the colliding ions rather than the fixed target scenario in Ref. [1], the estimate should be changed from the published $0.5/\gamma^2$ to $1/\gamma$, which, however, is still a very small number.
[20] A. H. Sørensen, Nucl. Instr. Meth. B **230**, 12 (2005). The full citation for Ref. [2] in this paper is the review above [14].
[21] J. Lindhard and A. H. Sørensen, Phys. Rev. A **53**, 2443 (1996).
[22] J. Beringer *et al.* (Particle Data Group), Phys. Rev. D **86**, 010001 (2012).
[23] J. Lindhard, Kgl. Danske Videnskab. Selskab, Mat. Fys. Medd. **34**(14), 1 (1965).
[24] A. H. Sørensen and E. Uggerhøj, Nucl. Sci. Appl. **3**, 147 (1989).
[25] A. H. Sørensen, in *Vacuum Structure in Intense Fields, NATO ASI Series B,* edited by H. M. Fried and B. Müller, Vol. 255 (Plenum, New York, 1991), p. 91; Nucl. Instr. Meth. B **119**, 1 (1996); **119**, 2 (1996). In the last article, page 19 should be read before page 17.
[26] P. A. Doyle and P. S. Turner, Acta Crystallogr. A **24**, 390 (1968).
[27] J. U. Andersen, E. Bonderup, E. Lægsgaard, B. B. March, and A. H. Sørensen, Nucl. Instr. Meth. **194**, 209 (1982).
[28] O. H. Nielsen and W. Weber, J. Phys. C: Solid State Phys. **13**, 2449 (1980).
[29] M. Abramowitz and I. A. Stegun (eds.), *Handbook of Mathematical Functions* (Dover, New York, 1972).